Sub-daily sea ice motion and deformation from RADARSAT observations

Ron Kwok and Glenn F. Cunningham
Jet Propulsion Laboratory, California Institute of Technology, Pasadena, California, USA

William D. Hibler III
IARC/Frontier, University of Alaska, Fairbanks, Alaska, USA

Received 26 September 2003; revised 21 October 2003; accepted 28 October 2003; published 11 December 2003.

[1] We find a persistent level of oscillatory sea ice motion and deformation, superimposed on the large-scale wind-driven field, in May 2002 (spring) and February 2003 (mid-winter), in the high Arctic over a region centered at ~(85°N, 135°W). At this latitude, the RADARSAT wide-swath SAR coverage provides 4–5 sequential observations every day, for ice motion retrieval, with a sampling interval at the orbital period of ~101 minutes. Periodic correlations in ice motion and deformation can be seen in length scales from 10 km and above, and suggest a 12-hr oscillation that is more likely associated with inertial rather than tidal frequencies. Divergence/convergence of ~0.1–0.2% peak-to-peak or rates of $\sim 10^{-7}$/s is seen in both datasets, with the mid-winter dataset having smaller values. These observations are remarkable in that short-period ice motion is previously believed to be inhibited by the strength of the ice pack in the high Arctic during winter. New ice production due to the recurrent openings and closings at these temporal scales, if ubiquitous, could be significant within the winter pack. *INDEX TERMS:* 4207 Oceanography: General: Arctic and Antarctic oceanography; 4540 Oceanography: Physical: Ice mechanics and air/sea/ice exchange processes; 4508 Oceanography: Physical: Coriolis effects. **Citation:** Kwok, R., G. F. Cunningham, and W. D. Hibler III, Sub-daily sea ice motion and deformation from RADARSAT observations, *Geophys. Res. Lett.*, *30*(23), 2218, doi:10.1029/2003GL018723, 2003.

1. Introduction

[2] Subdaily inertial motions in sea ice, during the Arctic summer, were first described by *Hunkins* [1967] and were subsequently studied by *McPhee* [1978] and *Colony and Thorndike* [1980]. *McPhee* [1978] further observed that these short-period variabilities disappeared almost entirely after freeze-up, yet *Hibler et al.* [1974] observed winter ice deformation with a 12-hr period. A recent investigation by *Heil and Hibler* [2002] of ice motion and deformation from contemporary buoy measurements shows substantial high-frequency variability at subdaily timescales over all seasons. However, buoy observations, typically separated by several hundred kilometers, are poor for understanding short length-scale motion and deformation. Here, we examine this phenomenon with high-resolution repeat coverage from RADARSAT SAR imagery with the objective of providing a more detailed look at the characteristics of these subdaily ice motion and deformation.

0094-8276/03/2003GL018723$05.00

2. Data Description

[3] Short-period ice motion and deformation estimates are derived from sequential RADARSAT imagery. The high frequency repeat imaging of a region of the ice cover takes advantage of the coverage overlap afforded by the RADARSAT wide-swath (460 km) SAR mode and the convergence of the satellite ground-tracks at high Arctic latitudes. At ~85°N, the westward precession of the orbit track allows 4–5 sequential observations every day with a sampling interval at the orbital period of ~101 minutes. The limitation is that this does not give us an entire daily cycle of motion observations as there is a ~16-hour gap until the next set of samples a day later.

[4] With this sampling scheme, we acquired RADARSAT coverage of an area (~200 km by 200 km) in the Canada Basin (centered ~85°N and 135°W) in May 2002 (Day 134–156) and February 2003 (Day 33–56) (Figure 1). The duration of each period is ~22 days. Lagrangian ice motion, giving the trajectory of each grid point, is derived on a 5 km initially uniform grid using the techniques described in *Kwok* [1998]. The Cartesian grid is defined on a co-ordinate system with 45°E and 135°E meridians as the abscissa and ordinate axes. Analysis of the RADARSAT imagery shows that over 98% of the area is covered by multiyear ice.

3. Results and Discussion

[5] The number of grid cells defined within each of the ice parcels and their associated temporal samples are shown in Figure 1. Also shown are the trajectories of the two ice parcels; the portions with short-period samples and the gaps are indicated. The total length of the May trajectory in 2002 is more than twice that of the one in February 2003.

[6] The results for the two periods are summarized in Figures 2. Figures 2a and 2b show the daily geostrophic wind vector along with the average ice displacement vector, and the associated strain ellipses over each orbital period. Colors on the vectors and ellipses indicate the progression in time relative to the first short-period sample after each observational gap (~16 hrs). Blue is earliest followed by green, orange, and red. Gray arcs connecting the tips of the displacement vectors show the approximate radii of the rotational component. This graphic representation shows

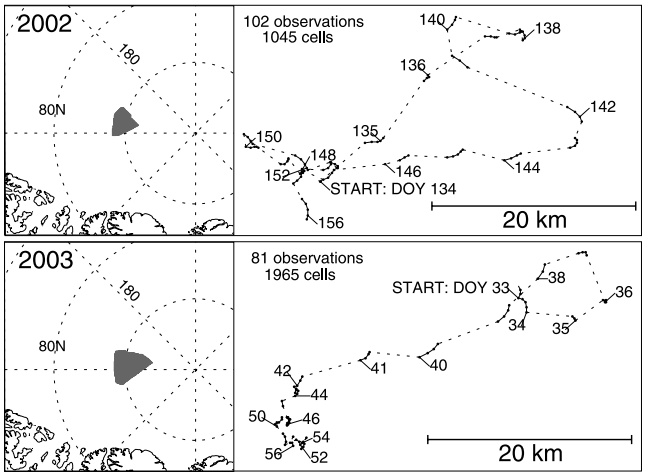

Figure 1. Trajectories of the two sample regions. (a) Day 134–156, 2002. (b) Day 33–56, 2003. Inset shows geographic location, and size and shape of each region. The initial location of both regions are centered at ~(85°N, 135°W) in the Beaufort Sea. Lines connect sequential observations (●). The number of 5 km cells within each region and the total number of observations over the period are shown.

the general coherent clockwise rotation of the ice motion vectors and the strain ellipses (discussed later).

[7] The strain ellipses are computed as follows. For a velocity field (*u, v*) in two dimensions, its strain rate can be written as,

$$\dot{\varepsilon} = \begin{pmatrix} \dfrac{\partial u}{\partial x} & \dfrac{1}{2}\left(\dfrac{\partial u}{\partial y} + \dfrac{\partial v}{\partial x}\right) \\ \dfrac{1}{2}\left(\dfrac{\partial u}{\partial y} + \dfrac{\partial v}{\partial x}\right) & \dfrac{\partial v}{\partial y} \end{pmatrix} \quad (1)$$

where $\partial u/\partial x$, $\partial u/\partial y$, $\partial v/\partial x$, $\partial v/\partial y$ are area-averaged spatial gradients in ice motion computed using a line integral around the boundary of the region. The strain over a time interval, Δt, can be visualized as a strain ellipse where an initial unit circle is rotated through an angle defined by the principal directions of $\dot{\varepsilon}\Delta t$ followed by stretching and contracting along these directions. With the principal values forming the length of the semi-major and semi-minor axes, the orientation of the ellipse shows the direction in which the greatest stretching occurred.

[8] All the motion samples are acquired around the same time of day, between 18Z and 02Z. In general, the vector displacements, as expected, rotate to the right of the daily geostrophic wind. Except for two days in May 2002 (Day 135 and 136), the clockwise rotations of the vectors are clearly discernible. Larger mean drift masks any small amplitude rotation in response to inertial or tidal forcing. Remarkable and perhaps unexpected is that the strain ellipses also rotate in a clockwise direction with the same phase during both periods. The rotation rates of the ellipses at 2.8π and 3.4π radians/day are consistent even though these rates are derived from a relatively short span ~0.6 of a semi-diurnal cycle.

[9] Figure 3 shows the four velocity gradients, divergence over a time step, and the fractional area change of the entire region relative to the first observation. There are fewer observations in 2003 even though it covered a larger area. The short-period velocity gradients also show remarkably similar behavior not just from day-to-day over each ~22-day period but also between both periods. Over each sub-period of 4–5 samples, the sequence of $\partial u/\partial x$ always increases with time, $\partial v/\partial x$ and $\partial u/\partial y$ show very distinct 'peaks', while $\partial v/\partial y$ shows dips. As there are fewer samples in Feb 2003, these repeating patterns are perhaps not as pronounced. The positive slope in divergence, $\partial u/\partial x + \partial v/\partial y$, over each sub-period is also evident. Divergence/convergence of ~0.1–0.2% or rates of $\sim 10^{-7}$/s during a 6-hr period is seen in both datasets, with the mid-winter dataset having smaller values. The fractional area change relative to the first data sample or net divergence shows larger longer-period divergent and convergent events, associated with wind-forcing, superimposed on the shorter-scale periodic behavior seen in the two time-series. The plots show clear coherent high-frequency oscillations in convergence/divergence, occurring at approximately same time of day.

[10] These results suggest an oscillatory motion and deformation behavior that has a near semi-diurnal period probably associated with inertial or tidal cycles. To examine the period of the oscillation, we compute the temporal correlation of the complex motion samples along the trajectories (Figure 2c). The real part of the function contains information on the lagged correlation of the x and y velocity components with itself while the imaginary part has information about the lagged correlation between the x and y components. If the velocity of an ice parcel undergoing a semi-diurnal oscillation has a positive x component at a certain time, it will have a negative y component 3 hours later. The imaginary part of the correlation should have negative peaks at 3 hrs, 15 hrs, etc. This is indeed observed in the datasets. Further, the lagged peaks of the imaginary part of the correlation function suggest that the oscillations are more likely 12-hrs as the locations of the peaks remain fairly constant after 4 days. At this latitude, the inertial period ($T = \pi/\omega \sin\theta$) is ~12 hrs. For oscillations due to semi-diurnal lunar tides (M_2 period = 12.42 hrs), the lagged peak at 4 days would have shifted by more than 3 hours and this is not evident here. However, this is not a clear diagnostic on the nature of these oscillations. An argument for inertial motion is that deformation associated with tidal motion caused by difference in phase of the tidal cycle at different points is small ($\sim 10^{-8}$/s) in the deep basins at length scales of ~100 km.

[11] Another interesting topic to examine is the length scale of the oscillatory deformation. To do this, we compute the temporal correlation of the strain and divergence at length scales of 10, 20, 40, and 80 km and areal extents of 100, 400, 1600, and 6400 km^2 (Figure 2c). The coherent oscillatory behavior of the correlations, associated with the semi-diurnal periods, is clearly evident in both datasets. It is intriguing that the periodic correlation peak magnitudes increase with length scale and areal extent. We speculate that this is due to the more random behavior of floes and lead orientations at the shorter length scales. At shorter length scales (<10 km), rigid floes are less likely to deform. We suspect that this is also likely to be thickness dependent.

[12] These recurrent openings and closings of pack ice during the winter, if ubiquitous, would increase the rate of

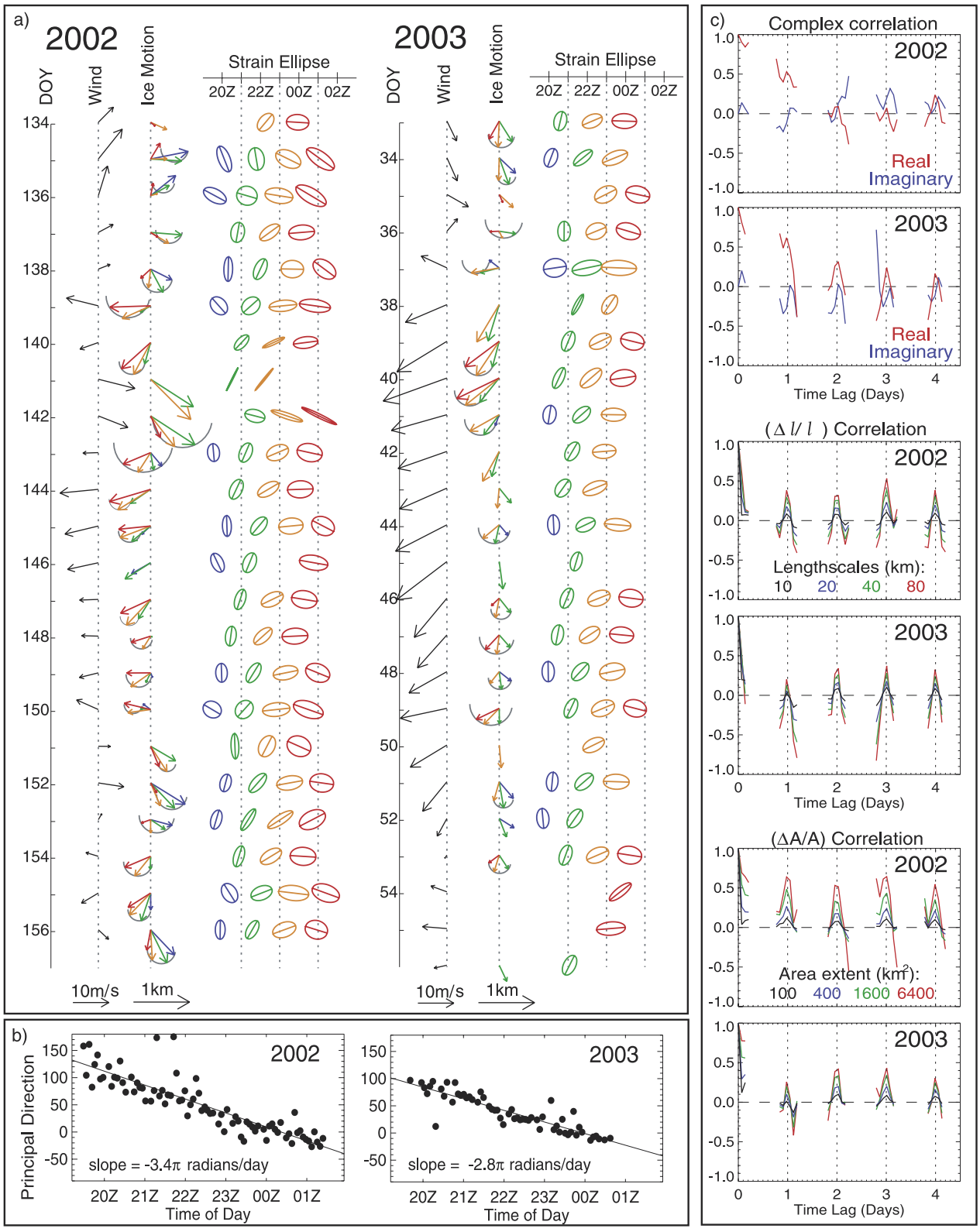

Figure 2. Characteristics of short-period ice motion and deformation during May 2002 (Day 134–156) and February 2003 (Day 33–56). (a) The geostrophic wind, ice motion, and strain ellipse associated each time step. Color of the vectors and ellipses (in the sequence of blue, green, orange, and red) are used to show progression in time. Sectors of circles (giving indication of radii) fitted to the motion vectors are shown in light gray. To visualize the biaxial strains, the principal values (defining the semi-major and minor axes of the ellipses) are exaggerated by a factor of 400. (b) The time dependence of the principal direction of the strain ellipses. (c) The temporal complex correlation of motion samples at all grid points, the temporal correlation of finite strain and divergence at the following length scales: 10 km, 20 km, 40 km, and 80 km, and the following areal extents: 100 km^2, 400 km^2, 1600 km^2, and 6400 km^2.

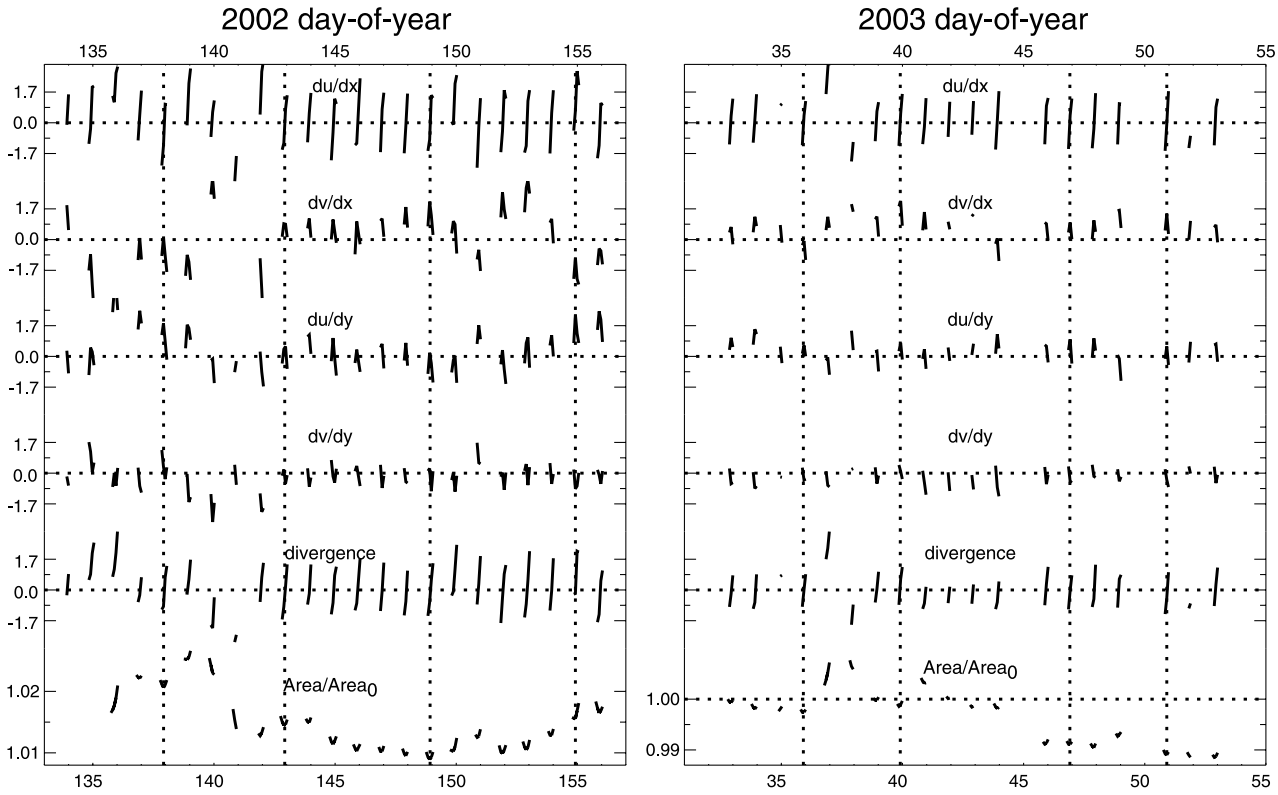

Figure 3. The four velocity gradients, divergence, and net area change computed over the two regions. (a) Day 134–156, 2002. (b) Day 33–56, 2003. Velocity gradients and divergence are in units of 10^{-7}/s.

ice production and have ramifications on the Arctic Ocean ice mass budget. A simple simulation of ice production (assuming a semi-diurnal oscillation with a 0.2% peak-to-peak divergence, ridging of all new ice, an air temperature of −25°C, and Lebedev's ice parameterization of ice growth) shows that this process can account for an equivalent of 10 cm of ice thickness over 6 months of winter. This is ∼20% of the basal ice growth of thick ice during the winter in the central Arctic (of ∼0.5 m).

4. Conclusions

[13] We have shown that semi-diurnal ice motion and deformation can be observed in high-resolution RADARSAT data. Both the May 2002 and February 2003 datasets exhibited similar oscillatory behavior over their entire ∼22-day periods, with the mid-winter dataset having smaller values of divergence and convergence. These observations are remarkable in that short-period ice motion is previously believed to be inhibited by the strength of the ice pack in the high Arctic during winter. The fact that this winter behavior of the ice cover, in response to inertial or tidal cycles, was not observed in earlier (<1970s) studies might perhaps be an indication of the recent thinning of the ice cover [*Rothrock et al.*, 2003].

[14] In any case, new ice production due to the recurrent openings and closings at these temporal scales, if ubiquitous, could be significant within the winter pack. A simple simulation of this process shows that it can account for an equivalent of 10 cm of ice thickness over 6 months of winter, approximately ∼20% of the basal ice growth of thick ice in the central Arctic (of ∼0.5 m). As noted by *Heil and Hibler* [2002], current models of sea ice dynamics typically do not include processes at such small time scales. If these processes are indeed important over the entire Arctic basin, their contribution to the mass budget should be included in numerical simulations of Arctic ice/ocean/atmosphere interactions.

[15] **Acknowledgments.** Special thanks to Miles McPhee for useful comments on the draft manuscript. RADARSAT images were processed at the Alaska SAR Facility. RK and GFC performed this work at the Jet Propulsion Laboratory, California Institute of Technology under contract with the National Aeronautics and Space Administration.

References

Colony, R., and A. S. Thorndike, The Horizontal Coherency of the Motion of Summer Arctic Sea Ice, *J. Phys. Oceanogr.*, *10*(8), 1281–1289, 1980.

Heil, P., and W. D. Hibler, Modeling the high-frequency component of Arctic sea ice drift and deformation, *J. Phys. Oceanogr.*, *32*(11), 3039–3057, 2002.

Hibler, W. D., III., W. F. Weeks, A. Kovacs, and S. F. Ackley, Differential sea ice drift I: Spatial and temporal variations in sea ice deformation, *J. of Glacio.*, *31*(69), 437–455, 1974.

Hunkins, K., Inertial Oscillations of Fletchers Ice Island (T-3), *J. Geophys. Res.*, *72*(4), 1165, 1967.

Kwok, R., The RADARSAT Geophysical Processor System, in *Analysis of SAR data of the Polar Oceans: Recent Advances*, edited by C. Tsatsoulis and R. Kwok, 235–257, Springer Verlag, 1998.

McPhee, M. G., Simulation of Inertial Oscillation in Drifting Pack Ice, *Dyn. Atmos. Oceans*, *2*(2), 107–122, 1978.

Rothrock, D. A., J. Zhang, and Y. Yu, The arctic ice thickness anomaly of the 1990s: A consistent view from observations and models, *J. Geophys. Res.*, *108*(C3), 3083, 2003.

G. F. Cunningham and R. Kwok, Jet Propulsion Laboratory, California Institute of Technology, 4800 Oak Grove Drive, Pasadena, CA 91109, USA. (ron.kwok@jpl.nasa.gov)

W. D. Hibler III, IARC/Frontier, University of Alaska, Fairbanks, Alaska, USA.